American Journal of Neural Networks and Applications
2026, Vol. 12, No. 2, pp. 57–75
https://doi.org/10.11648/j.ajnna.20261202.12

SciencePG
Science Publishing Group

Research Article

LIMD: LBP-InceptionV3 Hybrid Approach for Mpox Detection Using Skin Lesion Images

Vivian Ifeoma Nlemedim[1], Adetokunbo MacGregor John-Otumu[1,*], Nkechi Faustina Esomonu[1], Ferguson Ogene[2]

[1]Department of Information Technology, Federal University of Technology, Owerri, Nigeria

[2]Department of Computer Science & Information Technology, Petroleum Training Institute, Effurun, Nigeria

Abstract

Mpox skin lesions may exhibit visual similarities with other infectious skin conditions, particularly chickenpox and measles, making reliable image-based differentiation challenging. This study presents an LBP InceptionV3 hybrid approach for Mpox detection using skin lesion images. The proposed framework combines high level visual representations extracted using pretrained InceptionV3 with complementary local texture information generated using Local Binary Pattern (LBP). The secondary dataset comprised 228 original images. 102 images belong to Mpox class, while 126 images belong to the others class (chickenpox and measles). The images were expanded through augmentation to 3,192 images comprising 1,428 Mpox and 1,764 Other images. Images were standardized to 224 × 224 pixels and divided into training, validation, and testing sets using a 70:15:15 ratio. InceptionV3 generated a 2,048-dimensional deep feature representation, while LBP texture maps were processed through a shallow convolutional network to obtain 512 texture features. The resulting 2,560-dimensional representation was fused for classification. The proposed model achieved 94.15% accuracy, 94.16% precision, 94.15% recall, 94.16% F1 score, and an AUC of 0.99. On the 479 image test set, 451 images were correctly classified, including 202 Mpox and 249 Other images. The ablation study demonstrated that incorporating LBP improved accuracy from 88.72% for InceptionV3 alone to 94.15%, representing a 5.43 percentage point improvement, while AUC increased from 0.95 to 0.99. In addition, clinically sourced images from Owerri General Hospital were used to provide an independent assessment of the model on previously unseen skin lesion samples. The findings demonstrate that combining deep visual and local texture representations provides an effective approach for Mpox skin lesion classification.

Keywords

Mpox Detection, Local Binary Pattern, InceptionV3, Skin Lesion Classification, Deep Learning, Texture Features

1. Introduction

Infectious viral diseases that produce visible skin lesions remain an important public health concern, particularly when different diseases produce similar dermatological features. Mpox, chickenpox, and measles can all present with rashes, vesicles, papules, or other skin eruptions, making visual dif-

*Correspondence: Adetokunbo MacGregor John-Otumu (adetokunbo.johnotumu@futo.edu.ng)

Received: 5 September 2026; **Accepted:** 15 September 2026; **Published:** 28 September 2026

ferentiation difficult, especially during the early stages of infection [1].

Mpox has become particularly important because its clinical presentation can overlap with other infectious diseases. Mpox was traditionally found mainly in parts of West and Central Africa, but recent outbreaks have shown that the disease can spread beyond these regions. Chickenpox and measles, in comparison, occur worldwide. Although vaccination programmes have greatly reduced the number of cases in many areas, outbreaks can still occur, especially where vaccination coverage is low [13, 14].

Mpox can spread through close physical contact, respiratory droplets, and, in some outbreaks, intimate or sexual contact [5]. Chickenpox and measles are more easily transmitted, spreading mainly through airborne respiratory droplets and direct contact with an infected person [15, 16].

The lesions associated with Mpox commonly progress through stages that include macules, papules, vesicles, pustules, and scabs, while chickenpox and measles have their own characteristic patterns of lesion development and distribution.

These differences provide useful visual information, but the similarities can still make reliable classification difficult when assessment depends mainly on visual inspection. [1, 6]. Table 1 outlined the key clinical and rash differences among Mpox, chickenpox, and measles, while Figure 1 depicts the visual similarities and differences among Mpox, chickenpox, and measles skin lesions.

Table 1. *Key Clinical and Rash Differences Among Chickenpox, Monkeypox, and Measles.*

Feature	Chickenpox	Monkeypox	Measles
Causative Virus	Varicella-zoster virus	Monkeypox virus	Measles virus
Contagiousness	Highly contagious	Less contagious	Highly contagious
Initial Symptoms	Fever, headache, fatigue	Flu-like symptoms	High fever, cough, red eyes
Rash Appearance	Itchy, “dew drops on rose petals”	Macules → papules → vesicles → pustules → scabs	Red blotchy patches, often merged
Rash Distribution	Chest, back, face	Face → body	Face → chest/back/limbs
Distinctive Features	Itchy blisters	Lymphadenopathy	Koplik spots in mouth
Recovery	1–2 weeks, mild cases	2–4 weeks, variable severity	~2 weeks
Vaccination	Varicella vaccine	Smallpox vaccine	MMR vaccine

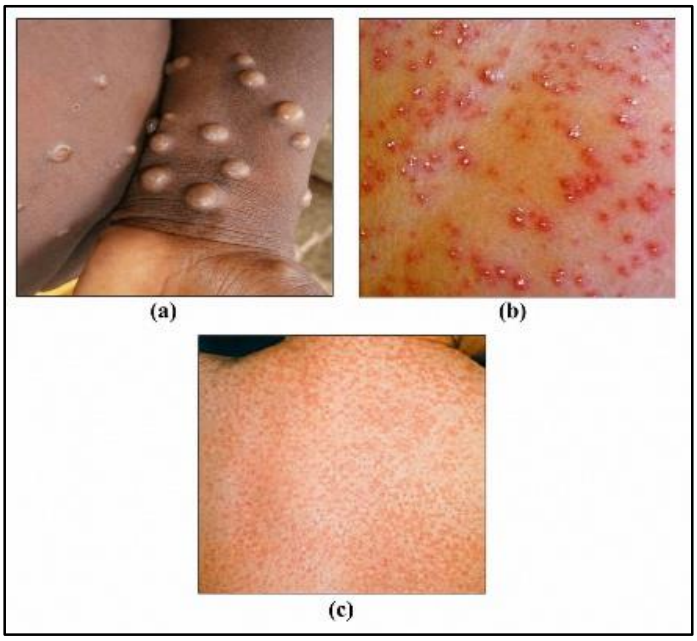

Figure 1. *Visual similarities and differences among Mpox, chickenpox, and measles skin lesions. (a) Sample Image of Mpox skin lesion (b) Sample Image of Chickenpox skin lesion (c) Sample image of a Measles skin lesion.*

Laboratory confirmation remains important for accurate Mpox diagnosis, but methods such as polymerase chain reaction can be costly, time consuming, and difficult to access in resource constrained settings, motivating the use of AI based image analysis for rapid decision support [1]. Ahsan et al. [2] reported 97% accuracy and 98% precision using modified VGG16, while Alrusaini [3] achieved 96% accuracy with VGG16. Islam et al. [4] reported 83% accuracy with VGG16 and 79% with InceptionV3. Despite these promising results, small datasets, web sourced images, limited clinical validation, and restricted demographic diversity may affect generalization [2-4]. In the present study, InceptionV3 achieved 88.72% accuracy in baseline testing [5]. To enhance its representation, Local Binary Pattern (LBP) was incorporated to capture fine local texture characteristics. The resulting hybrid approach combines InceptionV3's high level visual features with LBP based texture information to improve discrimination of Mpox from chickenpox and measles lesions.

2. Related Works

This section reviews existing studies on artificial intelligence based Mpox skin lesion classification, with emphasis on deep learning, hybrid architectures, attention mechanisms, and local texture representation. It examines the approaches, datasets, and reported performance of previous studies and highlights their key limitations. Particular attention is given to the challenges associated with limited datasets, image augmentation, restricted diversity, and inadequate external clinical validation. The section also establishes the motivation for combining InceptionV3 with Local Binary Pattern (LBP) to integrate high level visual features with complementary local texture information.

2.1. Deep Learning for Mpox Skin Lesion Detection

The application of artificial intelligence to infectious skin disease detection has expanded with the availability of digital skin lesion datasets and pretrained deep learning architectures. Early studies largely adopted transfer learning because of the limited availability of Mpox images [2-4].

Ahsan et al. [2] used a modified VGG16 model on 97 images and achieved 97% accuracy and 98% precision, although the small online dataset limits generalizability. Alrusaini [3] evaluated several pretrained architectures using 302 Google-sourced images, with VGG16 achieving 96% accuracy and a 92% F1-score. Islam et al. [4] developed an 804-image dataset covering several related conditions; VGG16, ResNet50, and InceptionV3 achieved 83%, 82%, and 79% accuracy, respectively. These studies demonstrate the potential of deep learning while highlighting the influence of dataset size, image source, and quality. They also suggest that backbone selection alone may be insufficient for capturing fine visual differences among related viral skin lesions.

2.2. Hybrid Approaches for Mpox Detection

Recent studies have increasingly explored hybrid architectures that combine multiple computational techniques for Mpox detection. Mandina and Murali [6] developed a Residual Attention U-Net with transfer learning and attention mechanisms, achieving 98% accuracy, although the study relied on augmented images and lacked real-time clinical evaluation. Shateri et al. [7] combined Xception, PCA, Natural Gradient Boosting, the African Vultures Optimization Algorithm, and LIME, achieving 92.6% accuracy, but was limited by a small dataset, augmentation dependence, and limited ethnic diversity. Devarajan et al. [8] combined a modified Restricted Boltzmann Machine, Equilibrium Optimizer, and CBAM, achieving 98.63% accuracy using an augmented 228-image dataset. However, external validation was not performed. These studies demonstrate the potential of hybrid approaches while highlighting a gap in combining handcrafted texture features with deep visual representations.

2.3. Attention-Based Deep Learning

Attention mechanisms have also been investigated as a means of improving the representation of relevant lesion characteristics. Haque *et al.* [5] combined transfer learning with CBAM and evaluated VGG16, ResNet50, and MobileNetV2 using a dataset containing 1,428 images. Their VGG16 model with attention achieved 84% accuracy and an F1-score of 83%. The study demonstrated that attention can improve feature discrimination, but it also reported limited diversity in skin tones and comparatively moderate performance.

The role of attention is different from that of texture representation. Attention mechanisms help a model emphasize informative feature channels or regions, whereas LBP explicitly represents local intensity relationships. The uploaded proposed architecture therefore treats these techniques as complementary rather than interchangeable.

2.4. Recent Deep and Hybrid Models

Recent research has produced increasingly high classification results. Saleh *et al.* [9] proposed a Swin Transformer, Particle Swarm Optimization, and SVM framework using 2,142 images obtained from open repositories. The system achieved 99.1% accuracy and 99.4% precision. The high results is based on the over reliance on web-scraped images and relatively high computational complexity, which may also affect practical deployment.

Kundu *et al.* [10] investigated federated deep learning using VGG16, ResNet50, and InceptionV3 together with CycleGAN-based synthetic image generation. Their VGG16-based federated model achieved 98.42% accuracy and 98.71% precision. The approach offers a privacy-preserving direction,

but the uploaded review identifies heavy reliance on synthetic data as well as possible communication and latency problems during deployment.

Waqar *et al.* [11] evaluated fine-tuned ConvNeXt architectures using an augmented dataset and reported 98.7% accuracy and a 98.6% F1-score for ConvNeXt Large. Vandana *et al.* [12] subsequently developed MRpoxNet using a modified ResNet50 and reported 98.1% accuracy. Both studies achieved strong results, but their dependence on augmented datasets and limited evaluation across different skin tones or lesion stages remain important concerns.

2.5. InceptionV3 and Local Texture Representation

Literature also showed that InceptionV3 has been used in previous Mpox classification studies, although it was not always the strongest-performing architecture. Islam *et al.* reported 79% accuracy for InceptionV3 [4].

The proposed use of LBP is motivated by the observation that skin lesions contain fine surface characteristics that complement global color, shape, and structural information. The LBP is applied to grayscale versions of the lesion images using 16 neighboring points and a radius of 2. The resulting maps are passed through a shallow CNN to learn discriminative texture representations.

2.6. Dataset Limitations and Generalization

A recurring issue across the reviewed studies is the limited size and diversity of original Mpox image datasets. Several investigations relied on fewer than 300 original images and subsequently increased the dataset through augmentation. The uploaded review notes that augmentation can increase the volume of training data but cannot fully reproduce real-world differences in skin tone, lesion stage, lighting, image quality, and clinical acquisition conditions.

The secondary dataset used in the uploaded study contains 228 original images, comprising 102 Mpox images and 126 images in the Other class, consisting of chickenpox and measles. An augmented version contains 3,192 images, comprising 1,428 Mpox images and 1,764 Other images. The images were standardized to 224 × 224 pixels for compatibility with the InceptionV3 architecture.

The study also includes an independent clinical dataset obtained from the Disease Surveillance Unit of Owerri General Hospital, Umuguma. It contains 15 Mpox images, 23 chickenpox images, and 22 measles images. These clinically sourced images were used to assess the model on previously unseen samples and provide an additional basis for examining practical generalization.

2.7. Research Gap and Positioning of the Present Study

The reviewed literature reveals five closely related gaps. First, many studies depend on small original datasets. Second, augmentation and synthetic data are frequently used to compensate for limited image availability. Third, several datasets are obtained from online sources without sufficient clinical standardization. Fourth, most existing systems emphasize deep feature learning without explicitly incorporating handcrafted texture descriptors. Finally, external validation using independent clinical images remains limited.

The present study addresses the fourth gap directly by combining InceptionV3 with LBP. InceptionV3 provides high-level semantic information concerning lesion structure, color distribution, and shape, while LBP provides a complementary representation of local texture. The two feature streams are processed separately and then fused before classification.

The empirical results support this design choice. The InceptionV3 + LBP configuration improved accuracy from 88.72% to 94.15%, showing that the addition of local texture representation produced a meaningful improvement over the single InceptionV3 model [5].

3. Materials and Methods

This section presents the materials and methods used in this study.

3.1. Materials

This subsection presents the various materials used, which includes the primary and secondary datasets, hardware as well as software specifications.

3.1.1. Dataset Source and Description

The section discusses the datasets used in this study as summarized in Tables 2 and 3.

Tables 2 and 3 present the sources, composition, and characteristics of the datasets used in this study. Table 2 shows that the primary dataset was obtained from the Disease Surveillance Unit of Owerri General Hospital, Umuguma, and contains 60 JPEG images across three classes: 15 Monkeypox, 23 Chickenpox, and 22 Measles images. Table 3 describes the secondary dataset obtained from Kaggle. It comprises 228 original images, including 102 Monkeypox and 126 Chickenpox and Measles images. The dataset was further expanded through augmentation to 3,192 images, consisting of 1,428 Monkeypox and 1,764 Other images. All secondary dataset images were standardized to 224 × 224 pixels to support the InceptionV3-based classification process. Together, the two datasets provided the basis for model development and validation.

Table 2. Source and Description of the Primary Dataset used in this study.

Item	Description
Original Primary Dataset Source	Owerri General Hospital, Umuguma (Disease Surveillance Unit) Owerri West, Imo State
Class	3 (Monkeypox, Chicken pox and Measles)
Samples in Monkeypox Class	15 Images
Samples in Chicken pox Class	23 Images
Samples in Measles Class	22 Images
Image Type	JPEG

Table 3. Source and Description of the Secondary Dataset Used in the Study.

Item	Description
Dataset Source (original images)	https://www.kaggle.com/code/mdismielhossenabir/monkeypox-skin-lesion/input?select=Original+Images
Dataset Source (Augmented Images)	https://www.kaggle.com/code/mdismielhossenabir/monkeypox-skin-lesion/input?select=Augmented+Images
Purpose of Dataset	Designed for classification of infectious viral skin lesions, with emphasis on Monkeypox and visually similar diseases such as Chickenpox and Measles
Dataset Composition	Consists of both original images and augmented images to improve model training and generalization
Total Dataset Size	Approximately 48.16 MB
Image Format	JPEG
Image Resolution	Standardized to 224 × 224 pixels to ensure compatibility with the InceptionV3 architecture
Number of Classes	Two classes: Monkeypox and Others (Chickenpox and Measles)
Original Dataset Size	228 clinically relevant skin lesion images
Monkeypox Images (Original)	102 images
Others Images (Original)	126 images consisting of Chickenpox and Measles
Purpose of Original Dataset	To provide real clinical visual patterns used as foundational data for model learning and validation
Augmented Dataset Size	3,192 images generated to increase dataset volume and diversity
Monkeypox Images (Augmented)	1,428 images
Other Images (Augmented)	1,764 images consisting of Chickenpox and Measles
Purpose of Augmented Dataset	Increased dataset variability in order to enhance the model's ability to learn robust and generalized feature representations

3.1.2. Experimental Setup

The section discusses the experimental setup used in this study.

Tables 4 and 5 present the hardware and software resources used to develop and implement the proposed system. Table 4 shows that the experiments were conducted on a Dell laptop with an Intel Xeon E3-1535M v6 processor running at 3.10 GHz, supported by 32 GB RAM and an NVIDIA GPU with 6 GB dedicated memory. The 1 TB HDD provided adequate storage for the datasets, models, and project files. Table 5 presents the software environment, which included Windows 11

(64-bit), Python 3.9.10, and Jupyter Notebook. Key libraries, including NumPy, Scikit-learn, TensorFlow, Matplotlib, Seaborn, and Flask, supported data processing, model development, evaluation, visualization, and system deployment. Together, these resources provided a suitable environment for implementing the proposed approach.

Table 4. Hardware Specification.

Component	Specification
Computer System	Dell Laptop
Processor	Intel Xeon E3-1535M v6
Processor Speed	3.10 GHz
Graphics Processing Unit (GPU)	NVIDIA GPU
GPU Memory	6 GB dedicated memory
RAM	32 GB
Storage	1 TB Hard Disk Drive (HDD)
Operating System	Windows 11, 64-bit
Processor Architecture	x64-based

Table 5. Software Specification.

Software /Tool	Version/Specification
Operating System	Windows 11, 64-bit
Programming Language	Python 3.9.10
Development Environment	Jupyter Notebook
Libraries	NumPy, Scikit-learn, TensorFlow, Matplotlib, Seaborn, Flask

3.2. Methods

This section presents the methods and procedures adopted to achieve the objective of the study. It describes the major stages involved in the development of the proposed LBP-InceptionV3 hybrid approach, including dataset preparation, image preprocessing, deep feature extraction using InceptionV3, texture feature extraction using Local Binary Pattern (LBP), feature fusion, model training, validation, and final performance evaluation. The section also explains how the extracted deep and texture features are combined and used for the classification of skin lesion images into Mpox and other visually similar viral skin conditions.

3.2.1. Proposed LBP-Inception V3 Framework

The section presents the proposed framework for detecting Mpox as illustrated in Figure 2.

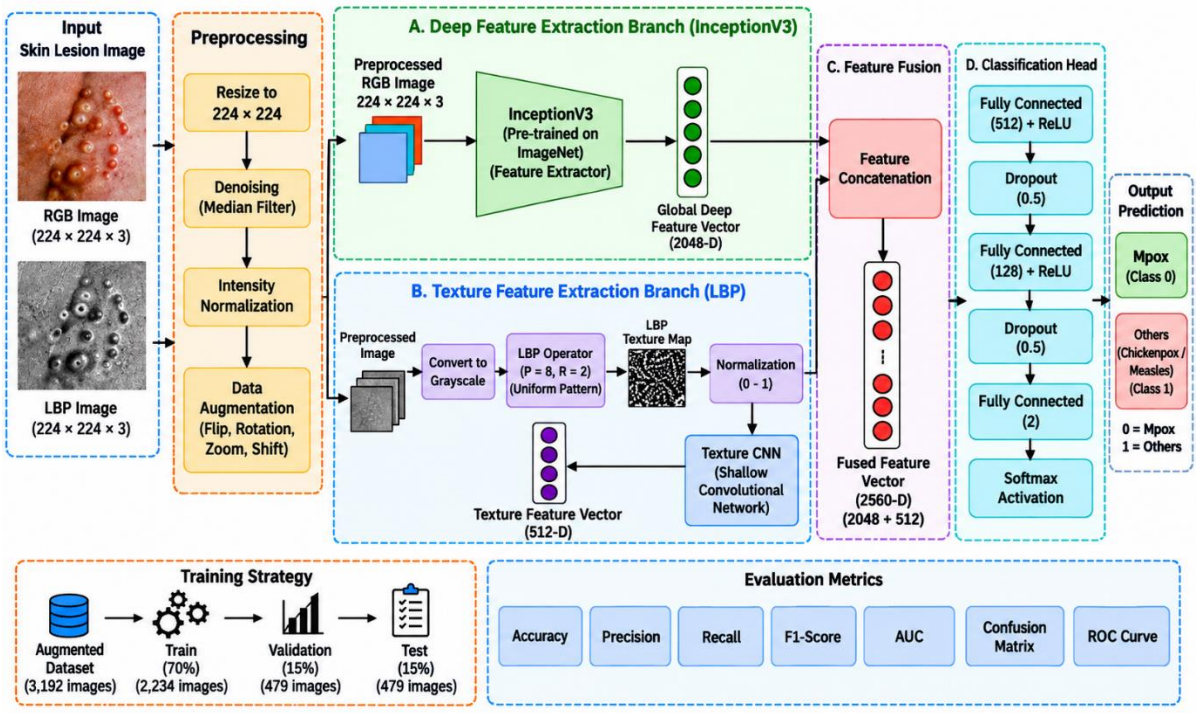

Figure 2. *Proposed LBP-InceptionV3 Hybrid Framework.*

Figure 2 presents the proposed framework for detecting Mpox from skin lesion images by combining deep visual features from InceptionV3 with texture features obtained using Local Binary Pattern (LBP). The framework begins with an RGB skin lesion image, which undergoes preprocessing involving resizing to 224 ×224 pixels, denoising with a bilateral filter, intensity normalization to the range of 0–1, and data augmentation through flipping, rotation, zooming, and shifting.

The preprocessed image is then processed through two parallel feature extraction branches. The first branch uses the pretrained InceptionV3 network as a deep feature extractor and produces a 2,048-dimensional deep feature vector. The second branch converts the image to grayscale and applies the LBP operator with $P = 16$ and $R = 2$ using a uniform pattern. The resulting texture map is normalized and passed through a shallow Texture CNN to generate a 512-dimensional texture feature vector.

The two feature vectors are subsequently concatenated to form a 2,560-dimensional fused feature vector. This combined representation is passed to the classification head, which consists of fully connected layers with 512 and 128 neurons, ReLU activation, and dropout of 0.5. A final fully connected layer with two outputs and softmax activation produces the classification probabilities for Mpox or Others (Chickenpox/Measles). For model development, the available data are divided into 70% training, 15% validation, and 15% testing. During training, the model performs forward propagation, loss computation, backpropagation, and parameter updating repeatedly across multiple epochs. The validation set is used to monitor performance, support hyperparameter tuning, early stopping, and model checkpointing. After training is completed, the unseen 15% test set is used for final evaluation using accuracy, precision, recall, F1-score, AUC, confusion matrix, and ROC curve. The trained model can subsequently be used to predict whether a new skin lesion image represents Mpox or another similar viral skin condition. The training parameters and hyperparameters are summarized in Table 6.

Table 6. *Training Parameters and Hyperparameters.*

Parameter / Hyperparameter	Value
Input image size	224 ×224 pixels
RGB input channels	3
LBP input channels	1
LBP number of sampling points (P)	16

Parameter / Hyperparameter	Value
LBP radius (R)	2
LBP method	Uniform
Batch size	16
Number of epochs	50
Learning rate	0.0001 (1×10^{-4})
Optimizer	Adam
Loss function	Binary Cross-Entropy
InceptionV3 pretrained weights	ImageNet
InceptionV3 include top	FALSE
InceptionV3 trainable	No (frozen)
RGB feature pooling	Global Average Pooling
LBP CNN Conv2D filters	32, 64
LBP CNN kernel size	3 ×3
LBP CNN activation	ReLU
LBP CNN padding (first Conv2D)	Same
LBP CNN pooling	MaxPooling2D
LBP CNN final feature pooling	Global Average Pooling
Fusion method	Concatenation
Fusion dense layer	256 neurons
Dense-layer activation	ReLU
Dropout rate	0.5
Output layer	1 neuron
Output activation	Sigmoid
Dataset split	70:15:15
Random state	42
RGB image normalization	Pixel values divided by 255.0
Evaluation metrics during training	Accuracy, AUC

3.2.2. Mathematical Formulation of the Proposed LBP-InceptionV3 Hybrid Framework

The proposed framework combines deep visual features extracted by InceptionV3 with texture features generated using Local Binary Pattern (LBP). The two feature representations are fused and passed to a fully connected classification network for binary classification of skin lesion images into Mpox and Others (Chickenpox/Measles). The mathematical formulation of the framework is presented below.

1) Image Preprocessing

Let the original RGB skin lesion image be represented by I. Each image is first resized to 224×224pixels to match the input requirement of the InceptionV3 network:

$$I_r = \text{Resize}(I, 224, 224) \quad (1)$$

The resized image is then denoised using a bilateral filter. The filtered image can be expressed as:

$$I_d(x) = \frac{1}{W_x}\sum_{y\in\Omega} G_s(\| x-y \|) G_r(| I_r(x) - I_r(y) |) I_r(y) \quad (2)$$

where G_s is the spatial Gaussian function, G_r is the range Gaussian function, Ω represents the local neighborhood, and W_x is the normalization factor.

Intensity normalization is subsequently applied to scale

pixel values to the range $[0, 1]$:

$$I_n = \frac{I_d - I_{\min}}{I_{\max} - I_{\min}} \quad (3)$$

Data augmentation, including flipping, rotation, zooming, and shifting, is then applied to increase the variation of the training samples.

2) Deep Feature Extraction Using InceptionV3

The normalized RGB image is supplied to the pretrained InceptionV3 network. The network acts as a feature extractor rather than the final classifier. The resulting deep representation is expressed as:

$$F_D = f_{\text{IncV3}}(I_n; \theta_D) \quad (4)$$

where f_{IncV3} represents the pretrained InceptionV3 feature extraction function and θ_D denotes its parameters. The resulting global deep feature vector has 2,048 dimensions:

$$F_D \in \mathbb{R}^{2048}$$

3) Texture Feature Extraction Using LBP

For the texture branch, the normalized image is converted to grayscale. For a central pixel g_c, the LBP value is calculated by comparing it with P neighbouring pixels g_p at radius R:

$$LBP_{P,R} = \sum_{p=0}^{P-1} s\left(g_p - g_c\right)2^p \quad (5)$$

where

$$s(z) = \begin{cases} 1, & z \geq 0 \\ 0, & z < 0 \end{cases}$$

In the proposed framework, $P = 16$ and $R = 2$. The resulting LBP texture map is normalized before being supplied to the shallow Texture CNN.

4) Texture Feature Extraction

The normalized LBP texture map is processed by the shallow convolutional network to obtain a compact texture representation:

$$F_T = f_{\text{CNN}}\left(L; BP_{16,2}\theta_T\right) \quad (6)$$

where f_{CNN} represents the Texture CNN and θ_T denotes its trainable parameters. The resulting texture feature vector contains 512 features:

$$F_T \in \mathbb{R}^{512}$$

5) Feature Fusion

The deep and texture feature vectors are combined through feature concatenation:

$$F_F = [F_D; F_T] \quad (7)$$

Therefore,

$$F_F \in \mathbb{R}^{2560}$$

since the fused representation contains 2,048 deep features and 512 texture features:

$$2048 + 512 = 2560$$

This fused representation allows the model to use both high-level visual information and local texture characteristics of the skin lesions.

6) Classification Head

The fused feature vector is passed to the first fully connected layer with 512 neurons and ReLU activation:

$$H_1 = \text{ReLU}(W_1 F_F + b_1) \quad (8)$$

where W_1 and b_1 are the weights and bias of the first fully connected layer.

Dropout with a rate of 0.5 is applied during training to reduce overfitting:

$$\tilde{H}_1 = M_1 \odot H_1 \quad (9)$$

where M_1 is a randomly generated dropout mask and $\odot$ denotes element-wise multiplication.

The resulting representation is passed to the second fully connected layer:

$$H_2 = \text{ReLU}\left(W_2 \tilde{H}_1 + b_2\right) \quad (10)$$

A second dropout operation with a rate of 0.5 is then applied:

$$\tilde{H}_2 = M_2 \odot H_2 \quad (11)$$

7) Softmax Prediction

The final fully connected layer contains two output neurons corresponding to Mpox and Others. The output logits are given by:

$$Z = W_3 \tilde{H}_2 + b_3 \quad (12)$$

The softmax function converts these logits into class probabilities:

$$P(y = k \mid X) = \frac{e^{Z_k}}{\sum_{j=1}^{2} e^{Z_j}} \quad (13)$$

where $k \in \{\text{Mpox}, \text{Others}\}$. The predicted class is the class having the highest probability:

$$\hat{y} = \arg\max_k P(y = k \mid X) \quad (14)$$

Thus, the model produces either Mpox (0) or Others (1) as

specified in the proposed architecture.

8) Loss Computation

For binary classification, the cross-entropy loss is used to measure the difference between the predicted probability and the actual class label:

$$\mathcal{L} = -\frac{1}{N}\sum_{i=1}^{N}\sum_{k=1}^{2} y_{ik}\log(\hat{y}_{ik}) \quad (15)$$

where N is the number of training samples, y_{ik} is the actual class label, and $\hat{y}_{ik}$ is the predicted probability for class k.

9) Backpropagation and Parameter Updating

The model parameters are updated by minimizing the loss through backpropagation. The general parameter update rule is:

$$\theta^{(t+1)} = \theta^{(t)} - \eta\nabla_{\theta}\mathcal{L} \quad (16)$$

where θ represents the trainable model parameters, η is the learning rate, and $\nabla_{\theta}\mathcal{L}$ represents the gradient of the loss with respect to the parameters.

This process is repeated over multiple training epochs using the 70% training data, while the 15% validation data are used to monitor model performance during training.

10) Model Evaluation

After training, the final 15% unseen test data are used to assess the model. Accuracy is calculated as:

$$Accuracy = \frac{TP+TN}{TP+TN+FP+FN} \quad (17)$$

Precision is given by:

$$Precision = \frac{TP}{TP+FP} \quad (18)$$

Recall is calculated as:

$$Recall = \frac{TP}{TP+FN} \quad (19)$$

and the F1-score is:

$$F1 = 2\left(\frac{Precision \times Recall}{Precision+Recall}\right) \quad (20)$$

where TP, TN, FP, and FN denote true positives, true negatives, false positives, and false negatives, respectively.

The model is further assessed using AUC, confusion matrix, and ROC curve to provide a broader assessment of its ability to distinguish Mpox lesions from Chickenpox and Measles lesions.

3.3. Proposed Algorithm

This section presents the computational steps of the proposed LBP-InceptionV3 hybrid algorithm, covering image preprocessing, parallel feature extraction, feature fusion, classification, training, validation, and testing for Mpox detection.

Algorithm 1: Proposed LBP-InceptionV3 Hybrid Framework for Mpox Detection

Input: Skin lesion image dataset D

Output: Trained hybrid model M, predicted class y, and evaluation results R

$$D_p \leftarrow \mathcal{P}(D)$$

where $\mathcal{P}$ represents image resizing to 224×224, bilateral filtering, normalization, and data augmentation.

$(D_{tr}, D_{val}, D_{te}) \leftarrow \text{Split}(D_p, 0.70, 0.15, 0.15)$.

For each image $x \in D_p$ do

$F_D \leftarrow f_{\text{IncV3}}(x)$.

$x_g \leftarrow \text{Grayscale}(x)$.

$L_x \leftarrow \text{LBP}(x_g; P; = 16R = 2)$.

$L_n \leftarrow \text{Normalize}(L_x)$.

$F_T \leftarrow f_{\text{TCNN}}(L_n)$.

$F_F \leftarrow [F_D; F_T]$.

End For

$\theta \leftarrow \text{Initialize}(\ )$.

For $e = 1, \ldots, E$ do

$z \leftarrow f_{\text{Cls}}(F_F; \theta)$.

$P \leftarrow \text{Softmax}(z)$.

$\mathcal{L} \leftarrow \text{Loss}(y, P)$.

$g \leftarrow \nabla_{\theta}\mathcal{L}$.

$\theta \leftarrow \text{Update}(\theta, g)$.

$V_e \leftarrow \text{Evaluate}(D_{val})$.

If V_e improves then

$M \leftarrow \text{SaveModel}(\theta)$.

End If
End For
$P_{te} \leftarrow M(D_{te})$.
$R \leftarrow \text{Evaluate}(P_{te}, D_{te})$.
For each new image x_{new} do
$x_p \leftarrow \mathcal{P}(x_{new})$.
$F_D \leftarrow f_{\text{IncV3}}(x_p)$.
$F_T \leftarrow f_{\text{TCNN}}\left(\text{LBP}(x_p; 16; 2)\right)$.
$F_F \leftarrow [F_D; F_T]$.
$P \leftarrow M(F_F)$.
$y \leftarrow \arg\max_k P_k$.
End For
Return M, y, R.

4. Results

This section presents the results obtained from the implementation and evaluation of the proposed LBP-InceptionV3 hybrid approach for Mpox detection. It describes the generated LBP texture images and the key results obtained during the different stages of the study.

4.1. Image Generated by the LBP Method

This subsection presents the texture images generated using the Local Binary Pattern (LBP) method. The generated images highlight local texture patterns in the skin lesions and provide additional texture information for the proposed hybrid model represented in Figure 3.

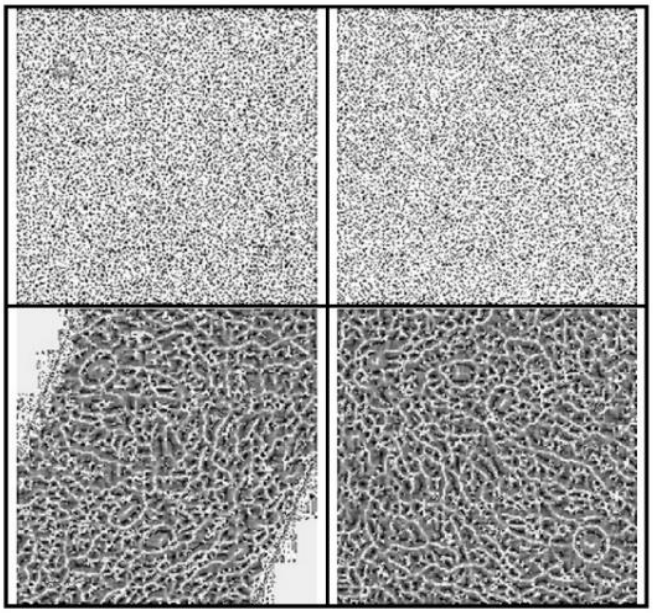

Figure 3*. Sample texturized Images generated by the LBP method.*

Figure 3 depicts the output of the Local Binary Pattern (LBP) feature extraction process, which converts skin lesion images into texture maps. The LBP method removes color information and focuses on local pixel intensity patterns, thereby highlighting fine texture details that may not be easily visible in the original RGB images. The generated texturized images capture important surface patterns, including fine-grained and structural features around the lesions. A total of 2,713 LBP-texturized images, representing 85% of the augmented dataset, were generated. These texture features complement the broader visual features extracted by InceptionV3, providing additional information that helps the hybrid model distinguish Mpox from visually similar skin conditions.

4.2. Training Results

This subsection presents the training results of the proposed LBP-InceptionV3 hybrid model. The results show the changes in training and validation accuracy and loss during model training as depicted in Figures 4 and 5. The ROC curve is also presented to assess the model's ability to distinguish between Mpox and the other skin conditions as depicted in Figure 6.

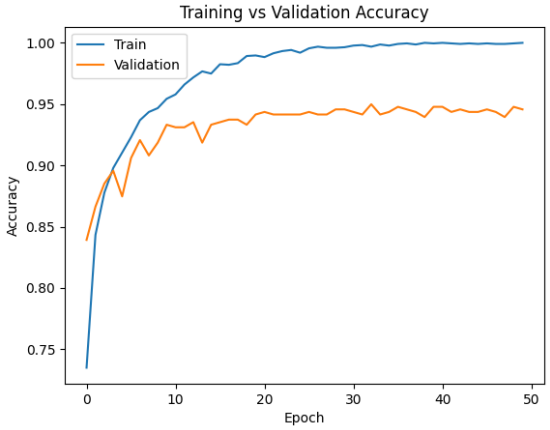

Figure 4. *Training/Validation Accuracy Curve.*

Figure 4 shows the training and validation accuracy of the proposed model over 50 epochs. The training accuracy increased steadily from approximately 73.5% in the first epoch to about 99.8%–100% by the final epochs. The validation accuracy also improved from about 84.0% initially, reaching approximately 92% around the sixth epoch and gradually stabilizing between 93% and 95% in the later epochs. At the end of training, the validation accuracy was approximately 94.5%, while the training accuracy was about 100%. The relatively stable validation performance indicates that the model learned useful patterns from the data, although the gap of about 5.5 percentage points between training and validation accuracy suggests some degree of overfitting.

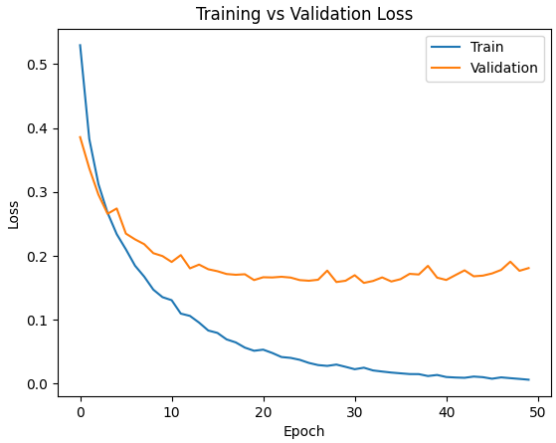

Figure 5. *Training/Validation Loss Curve.*

Figure 5 shows the training and validation loss of the proposed model over 50 epochs. The training loss decreased consistently from approximately 0.53 at the beginning of training to about 0.01 by the final epoch, indicating that the model progressively learned the patterns in the training data. The validation loss also decreased from about 0.38 to approximately 0.17 during the early stages of training. It reached its lowest value of around 0.16 between epochs 25 and 35, after which it showed small fluctuations and increased slightly to about 0.18 by the final epoch. The increasing gap between the training and validation losses in the later epochs suggests some degree of overfitting, while the relatively stable validation loss indicates that the model maintained reasonable performance on unseen data.

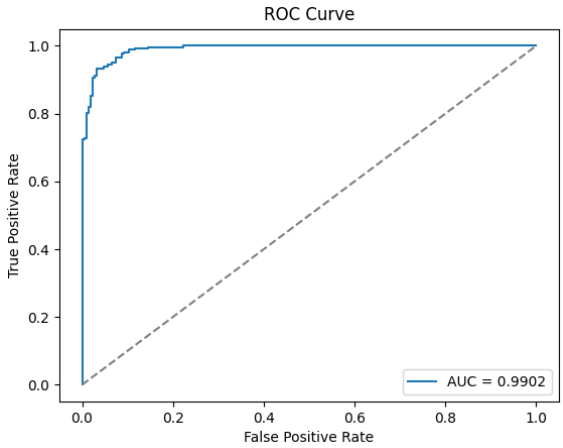

Figure 6. *ROC Curve.*

Figure 6 presents the Receiver Operating Characteristic (ROC) curve of the proposed model. The curve rises sharply toward the upper left corner, indicating a strong ability to distinguish between Mpox and the other skin lesion classes. The model achieved an Area Under the Curve (AUC) of 0.9902, which is very close to the maximum value of 1.0. This result shows that the proposed LBP-InceptionV3 hybrid approach has excellent classification capability, with a high true positive rate achieved at relatively low false positive rates. The ROC curve remains close to the top-left region before gradually reaching a true positive rate of 1.00, demonstrating the model's strong discriminative performance.

4.3. Confusion Matrix

This subsection presents the confusion matrix results of the proposed LBP-InceptionV3 model on the test dataset. The matrix shows the number of correctly and incorrectly classified images for Mpox and Others (Chickenpox and Measles), providing a clear view of the model's classification performance as depicted in Figure 7.

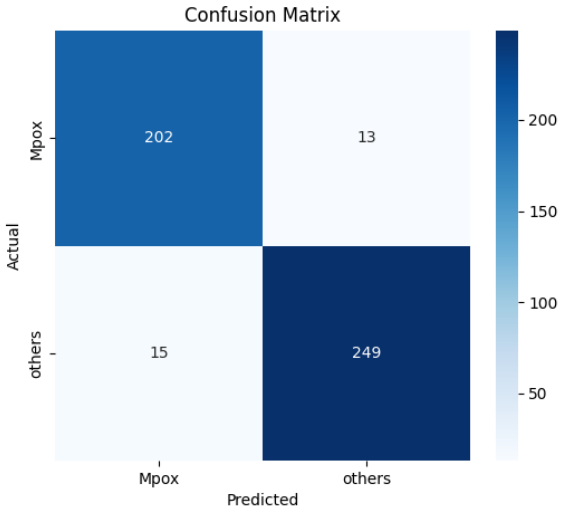

Figure 7. *LBP-Inception v3 Confusion Matrix.*

Figure 7 presents the confusion matrix of the proposed LBP-InceptionV3 model on the test dataset. The model correctly classified 202 Mpox images and 249 Others images, giving 451 correct predictions out of 479 test images. It incorrectly classified 13 Mpox images as Others and 15 Others images as Mpox. This corresponds to a classification accuracy of approximately 94.15%. For the Mpox class, the model achieved a precision of 93.09% and recall of 93.99%, while the F1-score was approximately 93.54%. The relatively small number of misclsassified images indicates that the proposed model was able to distinguish Mpox from Chickenpox and Measles effectively.

4.4. Classification Results of the Baseline and Proposed LBP-InceptionV3 Hybrid Deep Learning Model

This subsection presents the classification results obtained from the selected baseline model and the proposed LBP-InceptionV3 hybrid model. The results are compared using key performance measures to assess the effectiveness of combining deep visual features from InceptionV3 with texture features extracted using LBP as summarized in Table 7.

Table 7 presents the classification results of the selected baseline models using the augmented skin lesion dataset. The results show clear differences in performance among the models. The conventional CNN recorded the lowest performance, with an accuracy of 45.05%, precision of 54.60%, recall of 45.05%, and F1-score of 29.14%. ResNet50 performed better, achieving 55.42% accuracy, while VGG-16 recorded 70.64% accuracy and an F1-score of 69.83%. InceptionV3 showed a substantial improvement, achieving 88.72% accuracy, 88.73% precision, 88.72% recall, and 88.70% F1-score. The proposed InceptionV3 + LBP combination produced the best results, achieving 94.15% accuracy, 94.16% precision, 94.15% recall, and 94.16% F1-score. These results indicate that adding LBP texture features to InceptionV3 improved classification performance compared with the baseline InceptionV3 model.

Table 7. *Classification Results of the Selected Baseline Model on the Augmented Skin Lesion Dataset.*

Model	Accuracy	Precision	Recall	F1-Score
CNN	45.05	54.60	45.05	29.14
ResNet50	55.42	56.29	55.42	55.51
VGG-16	70.64	71.12	70.64	69.83
Inception v3	88.72	88.73	88.72	88.70
Inception v3 + LBP	94.15	94.16	94.15	94.16

4.5. Ablation Study

This subsection presents the ablation study conducted to examine the contribution of LBP to the performance of the InceptionV3 based model. The results compare the baseline InceptionV3 model with the LBP InceptionV3 model using accuracy, precision, recall, F1 score, and AUC as summarized in Table 8.

Table 8 shows that adding LBP features substantially improved the performance of the InceptionV3 model. The baseline InceptionV3 achieved an accuracy of 88.72%, precision of 88.73%, recall of 88.72%, F1 score of 88.70%, and AUC of 0.95. After incorporating LBP, the LBP InceptionV3 model achieved 94.15% accuracy, 94.16% precision, 94.15% recall, 94.16% F1 score, and an AUC of 0.99. This represents an accuracy improvement of 5.43 percentage points and an AUC increase of 0.04. The results indicate that the addition of LBP provided useful texture information that strengthened the classification capability of the InceptionV3 based model.

Table 8. Ablation Study Results Showing the Impact of LBP on the Performance of InceptionV3-Based Model.

Model	Accuracy	Precision	Recall	F1-Score	AUC
Inception v3	88.72	88.73	88.72	88.70	0.95
LBP-Inceptionv3	94.15	94.16	94.15	94.16	0.99

4.6. Comparison of Performance Evaluation with Previous Studies

This subsection compares the proposed LBP-InceptionV3 model with previous Mpox skin lesion classification studies, focusing on performance metrics and the contribution of combining deep visual features with LBP-based local texture representation.

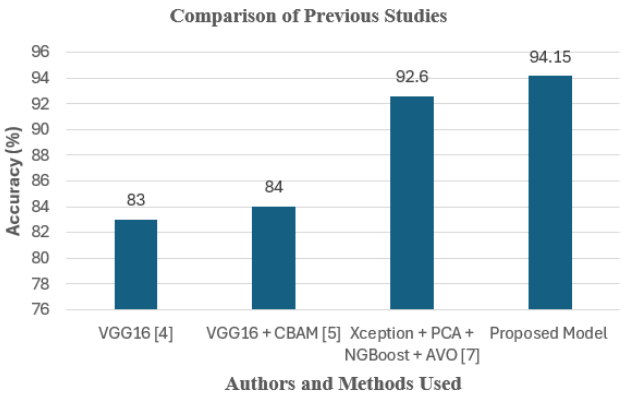

Figure 8. Comparison evaluation with Previous Studies.

Figure 8 presents a comparison of the proposed model with selected previous studies based on classification accuracy. The VGG16 model [4] achieved an accuracy of 83%, while VGG16 with CBAM [5] recorded 84%. The Xception + PCA + NGBoost + AVO + LIME approach [7] achieved a higher accuracy of 92.6%. In comparison, the proposed LBP-InceptionV3 model achieved 94.15% accuracy. The proposed model therefore outperformed VGG16 [4] by 11.15 percentage points, VGG16 + CBAM [5] by 10.15 percentage points, and the Xception-based approach [7] by 1.55 percentage points. These results indicate that the proposed integration of InceptionV3 deep features with LBP-based texture features provides better classification performance than the compared previous approaches. The result also shows that incorporating local texture information can improve the ability of the model to distinguish Mpox lesions from visually similar skin conditions.

4.7. Developed & Deployment of Web-based Prototype

A web-based prototype was developed using the proposed LBP-InceptionV3 model and Flask framework. The platform enables users to upload skin lesion images and obtain automated classification results for Mpox, chickenpox, and measles. The input and output interfaces are presented in Figures 9–11.

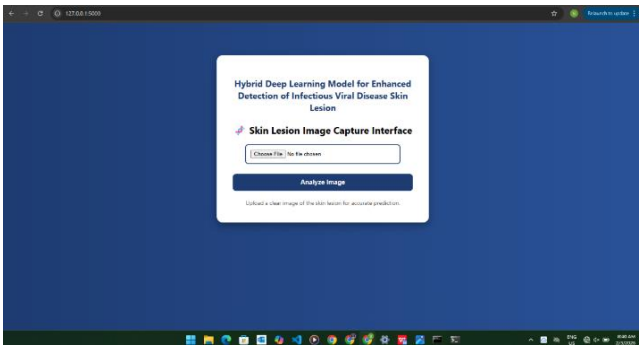

Figure 9. Developed Web-Based Input Interface for Skin Lesion Image Upload and Diagnostic Analysis.

Figure 9 illustrates the developed Web-Based Input Interface for Skin Lesion Image Upload and Diagnostic Analysis. The interface is accessed through the local host address 127.0.0.1:5000, indicating that the prototype is running on a local development server. The interface provides a "Skin Lesion Image Capture Interface" with a file-selection field for uploading a skin lesion image. After image selection, the "Analyze Image" button initiates the diagnostic analysis. The interface also provides an instruction indicating that the user should upload a clear image of the skin lesion for accurate prediction. The displayed screen therefore demonstrates the initial stage of the developed prototype, covering image selection and submission for automated analysis. No diagnostic classification result is displayed in Figure 9 because an image has not yet been selected and analyzed.

Figure 10. *Developed Web-Based Output Interface Displaying Diagnostic Prediction Result for Non-Mpox Skin Lesion.*

Figure 10 depicts the developed web-based output Interface displaying diagnostic prediction result for Non-Mpox Skin Lesion. The interface displays the predicted result as "Others", indicating that the uploaded skin lesion image was classified as a non-Mpox case. The displayed image provides the visual input used for the automated analysis, while the reported confidence level of 100.0% indicates that the model assigned complete confidence to the predicted Others class for this particular sample. The "Analyze Another Image" button provides an option to submit a different skin lesion image for further analysis. The result demonstrates the prototype's ability to present the model's classification outcome and corresponding confidence value through a simple web-based interface.

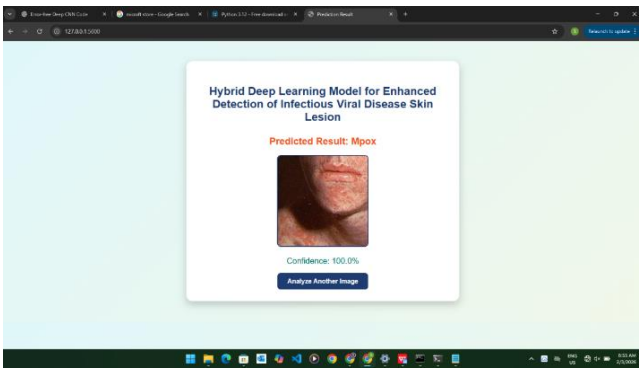

Figure 11. *Developed Web-Based Output Interface Displaying Diagnostic Prediction Result for Mpox Skin Lesion.*

Figure 11 depicts the developed web-based output interface for displaying diagnostic prediction result for Mpox Skin Lesion. The interface presents the uploaded skin lesion image with the predicted result identified as "Mpox." The model reports a confidence level of 100.0%, indicating complete confidence in assigning the displayed image to the Mpox class. The interface also provides an "Analyze Another Image" button, allowing users to submit additional images for automated classification. The result demonstrates the prototype's ability to display the predicted disease class together with its corresponding confidence value in a simple web-based format. Unlike Figure 10, where the prediction was "Others" with 100.0% confidence, Figure 11 demonstrates successful identification of an Mpox lesion with the same 100.0% confidence level, illustrating the prototype's ability to provide outputs for both classification categories.

4.8. Validation on Clinically Certified Images

This subsection evaluates the proposed hybrid model using unseen, clinically certified skin lesion images to assess its generalization beyond the experimental dataset. Table 9 presents 36 selected primary data images, comprising 12 each for Mpox, chickenpox, and measles, with ✓ indicating correct and ✗ indicating incorrect classification. The model correctly classified 9 of 12 Mpox images (75.00%), 8 of 12 chickenpox images (66.67%), and 11 of 12 measles images (91.67%), giving an overall classification rate of 77.78% (28/36). The results demonstrate the model's ability to recognize clinically obtained images, particularly measles, although misclassifications occurred between visually similar conditions, especially Mpox and chickenpox.

Compared with the 94.15% accuracy achieved on the experimental test set, the lower performance on clinical images highlights the importance of independent clinical validation. These findings provide preliminary evidence of practical potential but also indicate the need for larger and more diverse clinically certified datasets before stronger claims regarding clinical reliability or deployment can be made.

Table 9. *Web-based Hybrid Model integration for evaluation of primary data.*

Sample Images	Mpox	Chickenpox	Measles
Image-1	✓	✗	✓
Image-2	✓	✓	✓
Image-3	✓	✓	✓

Sample Images	Mpox	Chickenpox	Measles
Image-4	✓	✗	✗
Image-5	✓	✓	✓
Image-6	✗	✓	✓
Image-7	✓	✓	✓
Image-8	✓	✓	✓
Image-9	✗	✓	✓
Image-10	✓	✓	✓
Image-11	✗	✗	✓
Image-12	✓	✗	✓

* Legend: ✓ = Correctly classified; ✗ = Wrongly classified.

5. Discussion

This study investigated the effectiveness of combining deep visual features extracted using InceptionV3 with local texture information obtained through Local Binary Pattern (LBP) for Mpox skin lesion classification. The findings demonstrate that the proposed hybrid representation improved the performance of the standalone InceptionV3 model and achieved stronger performance than the baseline architectures evaluated on the same dataset. More importantly, the results provide experimental evidence supporting the central premise of the study: high level visual representations and local texture representations can provide complementary information for distinguishing Mpox lesions from visually similar chickenpox and measles lesions.

5.1. Principal Findings and Significance of the Proposed Approach

The proposed LBP InceptionV3 model demonstrated strong performance in distinguishing Mpox lesions from chickenpox and measles, achieving 94.15% accuracy, 94.16% precision, 94.15% recall, 94.16% F1 score, and 0.99 AUC. Of the 479 test images, 451 were correctly classified, including 202 Mpox and 249 Other images. Only 13 Mpox and 15 Other images were misclassified. The strength of the approach lies in combining complementary representations: InceptionV3 captures high level features such as lesion structure, color, and shape, while LBP captures fine local texture characteristics. Their fusion enhances the representation of discriminative lesion features. Compared with Islam et al. [4], where InceptionV3 achieved 79% accuracy, and the 88.72% baseline InceptionV3 result in this study, the improved performance demonstrates the value of incorporating LBP rather than relying solely on deep features.

5.2. Performance Improvement over Baseline Deep Learning Models

The baseline comparison demonstrates a clear improvement in classification performance. CNN, ResNet50, VGG16, and InceptionV3 achieved accuracies of 45.05%, 55.42%, 70.64%, and 88.72%, respectively, while the proposed InceptionV3 + LBP model achieved 94.15%, with 94.16% precision and F1-score and 94.15% recall. The strong performance of InceptionV3 is consistent with previous studies demonstrating the effectiveness of pretrained architectures for Mpox lesion classification. However, it differs from Islam et al. [4], who reported 79% accuracy for InceptionV3, and Alrusaini [3], where VGG16 achieved 96%. These variations highlight the influence of dataset characteristics, experimental conditions, and feature representation. The findings therefore suggest that, beyond backbone selection, enriching deep features with complementary texture information can further improve classification performance.

5.3. Contribution of LBP: Evidence from the Ablation Study

The ablation study provides clear evidence of the contribution of local texture information. InceptionV3 alone achieved 88.72% accuracy, 88.73% precision, 88.72% recall, 88.70% F1-score, and 0.95 AUC, while incorporating LBP increased these values to 94.15%, 94.16%, 94.15%, 94.16%, and 0.99, respectively. This represents a 5.43 percentage point improvement in accuracy and a 0.04 increase in AUC. The findings indicate that LBP complements InceptionV3 by capturing local intensity variations and fine texture patterns that may not

be fully represented by high-level deep features. This distinguishes the proposed approach from Shateri et al. [7], who combined Xception features with PCA, NGBoost, the African Vultures Optimization Algorithm, and LIME but did not incorporate handcrafted texture features, highlighting the value of complementary feature representation.

5.4. Comparison with Earlier Deep Learning Studies

The proposed model should be considered within the progression of earlier deep learning studies on Mpox detection. Ahsan et al. [2] reported 97% accuracy and 98% precision using a modified VGG16 model on 97 online images, while Alrusaini [3] achieved 96% accuracy using VGG16 on 302 digital images. In contrast, Islam et al. [4] reported 83% with VGG16, 82% with ResNet50, and 79% with InceptionV3 using an 804-image web-scraped dataset. The proposed 94.15% accuracy is lower than the results of Ahsan et al. [2] and Alrusaini [3], but higher than those of Islam et al. [4]. These differences should be interpreted cautiously, as dataset size, image source, quality, diversity, and clinical representativeness can substantially influence performance, particularly across varying skin tones, lesion stages, lighting, and acquisition conditions.

5.5. Comparison with Attention and More Complex Hybrid Approaches

Attention-based approaches provide a useful comparison. Haque et al. [5] combined transfer learning with CBAM and achieved 84% accuracy and 83% F1 score using VGG16. The proposed LBP InceptionV3 model therefore demonstrated higher performance, while employing a different feature enhancement strategy. Whereas CBAM emphasizes informative channels or regions, LBP explicitly captures local intensity relationships and texture patterns.

More complex hybrid approaches reported higher accuracies, including 98% by Mandina and Murali [6], 98.63% by Devarajan et al. [8], 99.1% by Saleh et al. [9], 98.42% by Kundu et al. [10], 98.7% by Waqar et al. [11], and 98.1% by Vandana et al. [12]. However, several relied on augmented or synthetic datasets and greater computational complexity. The proposed approach instead focuses on complementary texture representation, with the ablation study demonstrating a 5.43 percentage point accuracy improvement.

5.6. Comparison with the Xception Based Hybrid Approach

Shateri et al. [7] provides a relevant comparison because both studies employ hybrid strategies. Their approach combined Xception features with PCA, NGBoost, the African Vultures Optimization Algorithm, and LIME, achieving 92.6% accuracy on the 228 image Monkeypox Skin Lesion Dataset. In comparison, the proposed LBP InceptionV3 model achieved 94.15%, representing a 1.55 percentage point improvement. While the Xception based approach integrates dimensionality reduction, optimization, boosting, and explainability, the proposed model focuses on complementing deep visual features with local texture information. This finding suggests that meaningful performance gains can be achieved through feature complementarity without relying on highly complex hybrid configurations. However, the limitations noted by Shateri et al. [7], including small datasets, dependence on augmentation, and limited ethnic diversity, remain important considerations when interpreting Mpox classification performance.

5.7. Dataset Size, Augmentation and Generalization

Dataset size and augmentation are important considerations when interpreting the reported results. The secondary dataset contained 228 original images, comprising 102 Mpox and 126 Other images, and was expanded through augmentation to 3,192 images. While augmentation increased sample diversity, it cannot fully reproduce real-world variations in skin tone, lesion stage, lighting, image quality, and clinical acquisition conditions. Similar limitations were reported by Ahsan et al. [2], Alrusaini [3], Shateri et al. [7], Devarajan et al. [8], Waqar et al. [11], and Vandana et al. [12]. A key strength of the present study is the inclusion of previously unseen clinical images from Owerri General Hospital, comprising Mpox, chickenpox, and measles cases. However, the limited clinical sample size means that broader external validation is still required before general clinical validity can be established across diverse populations and imaging environments.

5.8. Clinical Relevance of the Findings

The ability to distinguish Mpox from chickenpox and measles is clinically important because these conditions may exhibit visually similar skin manifestations. The proposed model achieved 93.99% recall for Mpox, indicating that most Mpox images were correctly identified. However, the 13 false negative predictions demonstrate that misclassification remains possible. Therefore, the model should be considered a potential decision support tool rather than a replacement for laboratory confirmation. Image based AI could support rapid assessment, particularly where laboratory testing is costly, time consuming, or difficult to access.

5.9. Strengths, Limitations and Future Research

A major strength of the proposed approach is the clear contribution demonstrated through the ablation experiment. The improvement from 88.72% to 94.15% accuracy and from 0.95 to 0.99 AUC provides direct evidence that LBP contributed

useful information to the InceptionV3 representation. The use of both an augmented dataset and clinically sourced images also provides a stronger experimental basis than relying exclusively on a single source of online images.

However, the study shares some of the challenges identified in previous research. The number of original Mpox images remains limited, and augmentation cannot completely reproduce the diversity encountered in real clinical environments. The training behavior also indicates a degree of separation between training and validation performance at later stages, suggesting that the possibility of overfitting should be considered when interpreting the results.

Future work should therefore emphasize larger and more diverse clinically sourced datasets and stronger external validation. Particular attention should be given to variations in skin tone, lesion stage, lighting, image quality, and clinical acquisition conditions, which are repeatedly identified as important factors affecting the generalization of Mpox image classification systems.

6. Conclusions

This study developed and evaluated an LBP InceptionV3 hybrid framework for automated Mpox detection from skin lesion images. The model combines InceptionV3 for high level visual features with Local Binary Pattern (LBP) for local texture representation, providing complementary information for distinguishing Mpox from chickenpox and measles. The proposed model achieved 94.15% accuracy, 94.16% precision, 94.15% recall, 94.16% F1 score, and 0.99 AUC. On the 479 image test set, 451 images were correctly classified, including 202 Mpox and 249 Other images. The ablation study further demonstrated the contribution of LBP, with accuracy increasing from 88.72% for InceptionV3 alone to 94.15% after incorporating LBP, representing a 5.43 percentage point improvement.

Although the model outperformed the baseline CNN, ResNet50, VGG16, and standalone InceptionV3 models, comparisons with previous studies should consider differences in datasets, image sources, augmentation, architecture, and evaluation conditions. Importantly, evaluation on clinically sourced images produced a lower classification rate of 77.78%, highlighting the gap between experimental and real world performance.

The findings demonstrate the potential of the proposed framework as a supportive tool for Mpox assessment. However, it should not replace laboratory confirmation. Larger and more diverse clinically sourced datasets, independent external validation, and evaluation across different skin tones, lesion stages, lighting conditions, and imaging environments are recommended to establish broader generalizability and clinical applicability.

Abbreviations

AI	Artificial Intelligence
ANN	Artificial Neural Network
CBAM	Convolutional Block Attention Module
CNN	Convolutional Neural Network
ConvNeXt	Convolutional Next
InceptionV3	Inception Version 3
LBP	Local Binary Pattern
LIME	Local Interpretable Model-Agnostic Explanations
MMR	Measles, Mumps, and Rubella
ResNet50	Residual Network 50
VGG16	Visual Geometry Group 16
Xception	Extreme Inception

Acknowledgments

The authors would like to sincerely acknowledge Mrs. A. Chihoro, Disease Surveillance Officer at Owerri General Hospital, Umuguma, Owerri West, Imo State, for her valuable assistance in providing verified clinical samples used to validate this study. Her professional support and cooperation greatly contributed to the practical validation of the research. The primary image dataset used in this study was obtained from the Disease Surveillance Unit of Owerri General Hospital.

Author Contributions

Vivian Ifeoma Nlemedim: Conceptualization, Data curation, Methodology, Writing – original draft

Adetokunbo MacGregor John-Otumu: Formal Analysis, Investigation, Methodology, Supervision, Visualization

Nkechi Faustina Esomonu: Methodology, Supervision, Validation

Ferguson Ogene: Investigation, Methodology

Data Availability Statement

The original dataset that supports the findings of this study can be found at: https://www.kaggle.com/code/mdismielhossenabir/monkeypox-skin-lesion/input?select=Original+Images. While the augmented dataset can be found at: https://www.kaggle.com/code/mdismielhossenabir/monkeypox-skin-lesion/input?select=Augmented+Images

Conflicts of Interest

The authors declare no conflicts of interest.

References

[1] R. A. Farahat, R. Sah, A. A. El-Sakka, A. Y. Benmelouka, M. Kundu, F. Labieb, *et al.*, "Human monkeypox disease (MPX)," *Le Infezioni in Medicina*, vol. 30, no. 3, pp. 372–391, 2022, https://doi.org/10.53854/liim-3003-6

[2] M. M. Ahsan, K. A. Momin, M. R. Uddin, M. Farjana, A. N. Sakib, and S. A. Luna, "Image data collection and implementation of deep learning-based model in detecting monkeypox disease using modified VGG16," *arXiv preprint arXiv: 2206.01862*, 2022, https://doi.org/10.48550/arXiv.2206.01862

[3] O. A. Alrusaini, "Deep learning models for the detection of monkeypox skin lesion on digital skin images," *International Journal of Advanced Computer Science and Applications*, vol. 14, no. 1, pp. 637–644, 2023, https://doi.org/10.14569/IJACSA.2023.0140169

[4] T. Islam, M. A. Hussain, F. U. H. Chowdhury, and B. M. R. Islam, "A web-scraped skin image database of monkeypox, chickenpox, smallpox, cowpox, and measles," *arXiv preprint arXiv: 2209.00751*, 2022, https://doi.org/10.48550/arXiv.2209.00751

[5] M. E. Haque, R. S. Nila, M. R. Ahmed, and S. Islam, "Classification of human monkeypox disease using deep learning models and attention mechanisms," in *Proc. 25th Int. Conf. Computer and Information Technology (ICCIT)*, pp. 647–652, 2022.

[6] T. Mandina and P. Murali, "Intelligent deep learning based monkeypox detection," *Foundry*, vol. 28, no. 6, pp. 415–424, 2024.

[7] A. Shateri, N. Nourani, M. Dorrigiv, and H. Nasiri, "An explainable nature-inspired framework for monkeypox diagnosis: Xception features combined with NGBoost and African vultures optimization algorithm," *arXiv preprint arXiv: 2504.17540*, pp. 1–52, 2025, https://doi.org/10.48550/arXiv.2504.17540

[8] D. Devarajan, P. Dhana Lakshmi, S. Krishnaveni, and S. Senthilkumar, "Human monkeypox disease prediction using novel modified restricted Boltzmann machine-based equilibrium optimizer," *Scientific Reports*, vol. 14, no. 1, Art. no. 16252, 2024, https://doi.org/10.1038/s41598-024-67011-2

[9] H. Saleh, S. Mostafa, A. H. Ismail, S. Srivastava, and S. H. Alsamhi, "Swin-PSO-SVM: A novel hybrid model for monkeypox early detection," *IEEE Access*, vol. 12, pp. 187373–187385, 2024, https://doi.org/10.1109/ACCESS.2024.3513818

[10] D. Kundu, M. M. Rahman, A. Rahman, D. Das, U. R. Siddiqi, M. G. R. Alam, *et al.*, "Federated deep learning for monkeypox disease detection on GAN-augmented dataset," *IEEE Access*, vol. 12, pp. 32812–32829, 2024, https://doi.org/10.1109/ACCESS.2024.3370838

[11] M. Waqar, Z. A. Khan, S. T. Khawaja, N. I. Chaudhary, S. Khan, K. M. Cheema, *et al.*, "Explainable clinical diagnosis through unexploited yet optimized fine-tuned ConvNeXt models for accurate monkeypox disease classification," *SLAS Technology*, vol. 33, Art. no. 100336, 2025, https://doi.org/10.1016/j.slast.2024.100336

[12] V. Vandana, C. Sharma, and M. A. Shah, "MRpoxNet: An enhanced deep learning approach for early detection of monkeypox using modified ResNet50," *Digital Health*, vol. 11, pp. 1–18, 2025, https://doi.org/10.1177/20552076251320726

[13] Yuan, H., Yan, B., Chong, Y., Wang, L., & Jiang, Y. (2025). Time trend of measles burden on children and adolescents in BRICS-plus countries from 1990 to 2021 and prediction to 2032. Frontiers in Microbiology, 16, 1612124. https://doi.org/10.3389/fmicb.2025.1612124

[14] Kumar, K. (2023). Reservoir computing in epidemiological forecasting: Predicting chicken pox incidence. 1-17. medRxiv. https://doi.org/10.1101/2023.04.24.23289018

[15] Quach, H. Q., Jones, S. P., Joseph, I., Powell, A. J., Ovsyannikova, I. G., Warner, N. D.,... Kennedy, R. B. (2025). Low measles seropositivity in vaccinated children. JAMA Network Open, 8(1), e2452345. https://doi.org/10.1001/jamanetworkopen.2024.52345

[16] Wittenberg, R., Damant, J., Rehill, A., Knapp, M., Adeyemi, T., & Matthews, I. (2025). Estimated value of productivity lost due to childhood chickenpox in the United Kingdom: A survey of parents. *Expert Review of Pharmacoeconomics & Outcomes Research, 25(2), 197–203. https://doi.org/10.1080/14737167.2024.2410257

Research Field

Vivian Ifeoma Nlemedim: Machine Learning and Deep Learning

Adetokunbo MacGregor John-Otumu: Machine Learning, Deep Learning, Computer Vision, NLP, MAS, Intelligent Systems

Nkechi Faustina Esomonu: Data Science, AI, Machine Learning

Ferguson Ogene: Information Systems, Cybersecurity, Intelligent Networks, Machine Learning